IEEE Access
Multidisciplinary | Rapid Review | Open Access Journal

Received January 26, 2021, accepted February 23, 2021, date of publication March 9, 2021, date of current version March 30, 2021.

Digital Object Identifier 10.1109/ACCESS.2021.3064849

Vehicle Location in Edge Computing Enabling IoTs Based on Bistatic FDA-MIMO Radar

TENGXIAN XU[1,2], XIANPENG WANG[1,2], (Member, IEEE), TING SU[1,2], (Member, IEEE), LIANGTIAN WAN[3,4], (Member, IEEE), AND LU SUN[5]

[1]State Key Laboratory of Marine Resource Utilization in South China Sea, Hainan University, Haikou 570228, China
[2]School of Information and Communication Engineering, Hainan University, Haikou 570228, China
[3]Key Laboratory for Ubiquitous Network and Service Software of Liaoning Province, Dalian University of Technology, Dalian 116620, China
[4]School of Software, Dalian University of Technology, Dalian 116620, China
[5]Department of Communication Engineering, Institute of Information Science Technology, Dalian Maritime University, Dalian 116026, China

Corresponding authors: Xianpeng Wang (wxpeng1986@126.com) and Ting Su (suting4190@hainanu.edu.cn)

This work was supported in part by the Key Research and Development Program of Hainan Province under Grant ZDYF2019011, in part by the National Natural Science Foundation of China under Grant 61861015 and Grant 61961013, in part by the National Key Research and Development Program of China under Grant 2019CXTD400, in part by the Scientific Research Projects of University in Hainan Province under Grant Hnky2018ZD-4, in part by the Young Elite Scientists Sponsorship Program by the China Association for Science and Technology (CAST) under Grant 2018QNRC001, and in part by the Scientific Research Setup Fund of Hainan University under Grant KYQD(ZR)1731.

ABSTRACT Edge computing has a wide range of applications in the Internet of Things (IoT), especially suitable for low latency, high bandwidth, and high reliability. Edge computing enabling IoT can locate the vehicles rapidly with the help of edge computing. The sensors of IoTs can construct the Frequency diverse array (FDA) radar system, which has been widely concerned by scholars in recent years. The monostatic FDA and multiple-input-multiple-output (FDA-MIMO) is a research hotspot in parameter estimation field, but the research based on bistatic FDA-MIMO radar is insufficient. In this paper, we propose a tensor-based target location method in bistatic FDA-MIMO radar, which implements joint direction of arrival (DOA), direction of departure (DOD) and range parameters estimation. First of all, subarrays with different transmission frequency increment are used to construct the transmitting array to overcome the coupling between DOD and range. Then the tensor-based third-order signal model is established, which saves the multidimensional structure characteristics of received signal. And the signal subspace of each subarray is estimated by high-order-singular value decomposition (HOSVD). Furthermore, the phase period ambiguity is eliminated by limiting the range of the target, and the method for DOA, DOD and range parameters matching is provided. Theoretical analysis and numerical simulations demonstrate the effectiveness and superiority of the proposed method.

INDEX TERMS Internet of Things, bistatic FDA-MIMO radar, vehicle location, HOSVD.

I. INTRODUCTION

Edge computing can support unmanned driving, traffic flow diversion and congestion prediction, etc, in urban traffic through the real-time data processing and analysis functions of edge computing. The sensors of Internet of Things (IoT) can be deployed to locate the vehicles in Intelligent Transportation System. Thus edge computing enabling IoTs can locate the vehicles rapidly with the help of edge computing based on the sensors of IoTs [1]–[4], which can be constructed with the radar system. In order to achieve the vehicles location with the help of edge computing, high resolution parameter estimation, such as angle and rang, is the key issue in the radar system. Recently, multiple-input-multiple-output (MIMO) radar has attracted a lot of attention due to its unique advantages, such as high degrees of freedom (DOF) and parameter estimation accuracy [5]–[9]. In order to deal with complex and dynamic clutter, MIMO radar adopts flexible signal waveforms and array antenna configuration methods to obtain greater freedom [10], [11]. However, MIMO radar also has certain shortcomings. The beam pointing is not affected by the range, which also means that the beam pointing of the MIMO radar has no correlation with the range [12]. However, in some target positioning, range correlation is needed

The associate editor coordinating the review of this manuscript and approving it for publication was Chengpeng Hao.

to suppress clutter. The array beam is expected to point at different range with the same angle, which requires that the direction of the beam can change with different range [13].

Frequency diverse array (FDA) is a brand new institutional radar [14], which has been widely studied by scholars in the field of radar and navigation. Because it uses different transmission frequency on different elements of the transmitting array, the beam patern can be changed with range, so the array factor of the frequency array radar is range-dependent, and the range direction of the transmitting beam can be controlled [15]. FDA radar has many advantages, such as anti-clutter and anti-jamming [16]. Thus, it has a widely applications in the field of target positioning [17]–[19]. In [20], the FDA uses a double pulse method to estimate the parameters of targets. The frequency increments of the transmission are zero and non-zero, respectively. Then the traditional phased array method is used to achieve angle estimation, and the FDA scheme is used to achieve the target range estimation. In [21], some scholars proposed a method for estimating target positioning parameters using sub-array FDA. Specifically, the FDA consists of two sub-arrays, and their frequency incerments are different. The frequency of the traditional FDA radar increases linearly, and the division of sub-arrays essentially increases the frequency nonlinearly, which is an improvement of the traditional FDA radar. Besides, two new types of FDA radars is proposed in [17], [18]. One is random FDA array, and the other is relatively prime FDA array, both of which are with increasing frequency nonlinearity.

The combination of FDA and MIMO radar is a new type of decoupling method [22]–[24], which has attracted the research of many scholars. The FDA-MIMO radar makes full use of the freedom of transmission waveform and the freedom of beam distance pointing of the frequency-controlled array MIMO radar [25], [26]. At the same time, its wide and narrow gaze observation method can relax the standard for the dunamic range of the radar system, extend improve the observation time and the speed resolution of the target, thereby helping to store target energy and suppress clutter [16]. Currently, there are many angle estimation methods based on subspace [27]–[29]. One is to estimate signal parameters through the rotation invariance technique (ESPRIT) method in [30], and the other is the multiple signal classification (MUSIC) method in [31]–[33]. However, the spectral peak search of MUSIC and SVD of the ESPRIT method requires a lot of calculations, which increases the computational complexity of the method. The MUSIC method involves spectral peak search [34], and the complexity of the three-dimensional parameters estimation method for DOA, DOD and range is a very high challenge, which is not easy to implement in practical applications [35]. In addition, sparse DOA estimation methods are a very important category [36], [37]. The sparse Bayesian learning (SBL) method and l1-singular value decomposition (SVD) have been proposed in [8], [38], respectively. At present, the research of FDA-MIMO radar mainly focuses on the monostatic scenario, because the estimation of angle and range can be achieved by extending the method based on MIMO radar [35], [39], [40]. However, these methods can only be applied in the monostatic system, and they will fail in the face of bistatic FDA-MIMO radar. Thus, further research for parameter estimation in the bistatic FDA-MIMO radar is needed.

In this paper, we proposed a tensor-based method for joint estimation of DOA, DOA and range in bistatic FDA-MIMO radar with the subarray mode. Different frequency increment subarrays are used to construct the transmitting array, so that each subarray has rotation invariance for angle tstimation. First, we build a third-order signal model based on tensor to save the inherent multi-dimensional structural characteristics of the received signal,and then HOSVD is used to estimate the signal subspace of each subarray. Finally, the target parameters can be estimated by combining subspace-based method, and the phase period ambiguity can be eliminated by limiting the range of target. Moreover, because the proposed method uses the tensor-based received signal to save the inherent multi-dimensional structural characteristics of the data, the performance of the proposed method has been greatly improved compared with the traditional method based on matrix decomposition. The main contributions of this paper are summarized as follows:

(1) The proposed method implements the FDA-MIMO radar target location in the tensor domain. The tensor-based signal model saves the multi-dimensional structural information of the received signal, which can improve the accuracy of target location.

(2) The transmitting matrix and the receiving matrix of the receiving signal are extracted by rotation invariance, and the independent transmitting matrix of each sub-array is extracted by the selection matrix, so as to clearly obtain the coupling information of each subarray DOD and range parameters.

(3) The computational complexity of the proposed method is analyzed. And compared with traditional subspace-based method, the simulation results verify the superiority of the tensor-based target location method.

Notation : $\boldsymbol{\mathcal{X}}$ is denoted as a tensor. $\otimes$ stands for the Kronecker product and $\odot$ stands for the Khatri-Rao product. $\boldsymbol{I}_M$ indicates the $M \times M$ identity matrixes, and $\mathbf{0}_M$ and $\mathbf{0}_{M\times N}$ represent the zero matrices with dimensions $M \times M$ and $M \times N$, respectively. The conjugation, transpose and the conjugate-transpose of matrix can be expressed as $(\cdot)^H$, $(\cdot)^T$ and $(\cdot)^*$, respectively. Moreover, $(\cdot)^\dagger$ stands for the pseudo-inverse of matirx. And $\lfloor * \rfloor$ represent the floor operator. The $angle(*)$ stands for extraction phase.

II. TENSOR BASICS AND SIGNAL MODEL OF VEHICLE LOCATION

A. TENSOR BASICS

This section introduces some knowledge of tensor decomposition to help understand the operations of tensor algebra. For more related knowledge, please refer to [41], [42].

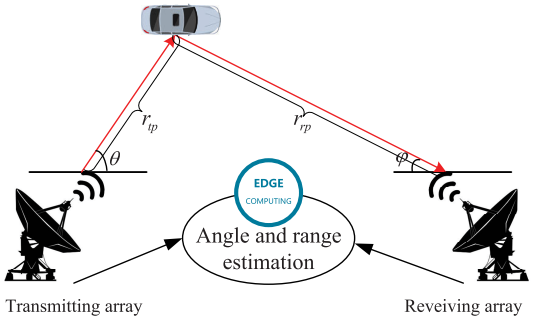

FIGURE 1. Edge computing enabling IoT for vehicle location system.

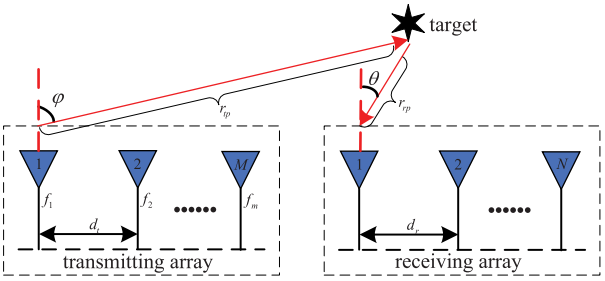

FIGURE 2. Bistatic FDA-MIMO radar.

*Definition 1 (Mode-*n *Tensor unfolding):* Let $\boldsymbol{\mathcal{X}} \in \mathbb{C}^{I_1 \times I_2 \cdots \times I_N}$ represents a tensor. The mode-n tensor unfolding of the tensor $\boldsymbol{\mathcal{X}}$ can be written as $[\boldsymbol{\mathcal{X}}]_{(n)}$. The element $(i_1, i_2 \cdots i_n)$ of tensor $\mathcal{X}$ corresponds to the (i_n, j)th element of $[\boldsymbol{\mathcal{X}}]_{(n)}$, where $j = 1 + \sum_{k=1,k\neq n}^{N}(i_k - 1)J_k$, and $J_k = \prod_{m=1,m\neq n}^{k-1} I_m$.

*Definition 2 (Mode-*n *tensor-matrixes product):* $\boldsymbol{\mathcal{Y}} = \boldsymbol{\mathcal{X}} \times_n \boldsymbol{A}$ represents the mode-n product of tensor $\boldsymbol{\mathcal{X}} \in \mathbb{C}^{I_1 \times I_2 \cdots \times I_N}$ with the matrixes $\boldsymbol{A} \in \mathbb{C}^{J_n \times I_n}$. It can be derived that $\boldsymbol{\mathcal{Y}} \in \mathbb{C}^{I_1 \times I_2 \times \cdots \times I_{n-1} \times J_n \times I_{n+1} \times \cdots \times I_N}$ and

$$[\boldsymbol{\mathcal{Y}}]_{i_1, i_2, \cdots, i_{n-1}, j_n, i_{n+1}, \cdots, i_N} = \sum_{i_n=1}^{I_n} [\boldsymbol{\mathcal{X}}]_{i_1, i_2, \cdots, i_{n-1}, i_n, i_{n+1}, \cdots, i_N} [\boldsymbol{A}]_{j_n, i_n} \tag{1}$$

Definition 3 (The properties of the mode product): The Mode-n tensor-matrixes product satisfies the following operational transformation rules

$$\begin{cases} \mathcal{X} \times_m \boldsymbol{A} \times_n \boldsymbol{B} = \mathcal{X} \times_n \boldsymbol{B} \times_m \boldsymbol{A}, m \neq n \\ \mathcal{X} \times_m \boldsymbol{A} \times_n \boldsymbol{B} = \mathcal{X} \times_n (\boldsymbol{BA}), m = n \end{cases} \tag{2}$$

Definition 4 (Tensor decomposition): The HOSVD of tensor $\boldsymbol{\mathcal{X}} \in \mathbb{C}^{I_1 \times I_2 \cdots \times I_N}$ is given by

$$\boldsymbol{\mathcal{X}} = \boldsymbol{\mathcal{G}} \times_1 \boldsymbol{U}_1 \times_2 \boldsymbol{U}_2 \times_3 \cdots \times_N \boldsymbol{U}_N \tag{3}$$

where $\boldsymbol{\mathcal{G}} \in \mathbb{C}^{I_1 \times I_2 \times \cdots \times I_N}$ represents the core tensor of $\boldsymbol{\mathcal{X}}$, and $\boldsymbol{U}_n \in \mathbb{C}^{I_n \times I_n} (n = 1, 2, \cdots, N)$ is a unitary matrixes that composed of the left singular vector of $[\boldsymbol{\mathcal{X}}]_{(n)}$.

B. TENSOR-BASED SIGNAL MODEL

Edge computing enabling IoT for vehicle location system is shown in Figure 1, the sensors IoTs are constructed with bistatic FDA-MIMO radar system. The parameters, such as DOD, DOA and range, are the key issue for vehicle location, because the location of vehicle can be achieved by combing the information of angle and range, which is shown in Figure 2. Thus, we focus on the parameter estimation for bistatic FDA-MIMO radar. Consider the bistatic FDA-MIMO radar with a narrow-band and wide beam, which is equipped with M transmitting antennas and N receiving antennas. Both of the transmitting array and receiving array are configured by uniform linear arrays (ULA), which spacing of them are denoted by d_t and d_r, respectively. Select the frequency of the first transmitting antenna, generally called the initial frequency, the transmission frequency of the mth transmitting antenna is written by

$$f_m = f_1 + (m-1)\Delta f, \quad m = 1, 2, \cdots, M \tag{4}$$

where f_1 stands for the initial frequency, and Δf is the increase in frequency of adjacent transmitting antennas, and $\Delta f \ll f_1$.

The signal transmitted that is narrow-band complex from the mth array antenna can be expressed as

$$s_m(t) = \phi_m(t) e^{j2\pi f_m t}, 0 \leq t \leq T \tag{5}$$

where T stands for the radar pluse duration, and $\phi_m(t)$ repersents the baseband signal of antenna. We define that the waveforms are orthogonal to each other, which can be written as

$$\int_0^{\mathrm{T}} \phi_m(t) \phi_n^*(t-\tau) e^{j2\pi \Delta f (m-n)t} dt = \begin{cases} 0, & m \neq n, \forall \tau \\ 1, & m = n, \tau = 0 \end{cases} \tag{6}$$

where the time shift is τ. We preset P far-field targets, and they are non-coherent to each other. Then for the pth target, the received signal of nth receiving antenna is written by

$$x_n(t) = \sum_{m=1}^{M} \beta_p \phi_m \left(t - \tau_{m,p}^t - \tau_{n,p}^r\right) e^{j2\pi f_m \left(t - \tau_{m,p}^t - \tau_{n,p}^r\right)} \tag{7}$$

where β_p stands for the complex reflection coefficient of the pth target, the transmitting time delays and receiving time delays is denoted by $\tau_{m,p}^t$ and $\tau_{n,p}^r$, respectively.

The direction of arrival and direction of departure of the pth target are denoted as θ_p and φ_p, respectively. c stands for speed of light and $c = 3 \times 10^8 m/s$. Then we can get

$$\begin{aligned} \tau_{m,p}^t &= \left(r_{1,p}^t - (m-1) d_t \sin\left(\theta_p\right)\right)/c \\ \tau_{n,p}^r &= \left(r_{1,p}^r - (n-1) d_r \sin\left(\varphi_p\right)\right)/c \end{aligned} \tag{8}$$

The receiver and transmitter steering vectors for the kth target can be expressed as

$$\boldsymbol{a_r}(\theta_p) = [1, e^{j2\pi f_1 d_r \sin(\theta_p)/c}, \cdots, e^{j2\pi (N-1) f_1 d_r \sin(\theta_p)/c}]^{\mathrm{T}} \tag{9}$$

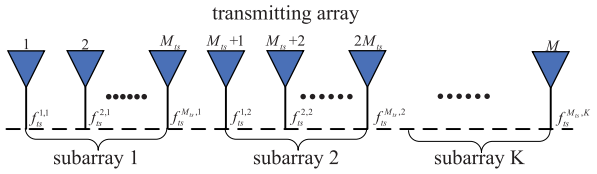

FIGURE 3. Subarray model transmitting array.

$$\boldsymbol{a}_t\left(r_p,\varphi_p\right)=\begin{bmatrix}1\\ e^{j\frac{2\pi}{c}\left(d_tf_1\sin(\varphi_p)-\Delta fr_p\right)}\\ \vdots\\ e^{j(M-1)\frac{2\pi}{c}\left(d_tf_1\sin(\varphi_p)-\Delta fr_p\right)}\end{bmatrix}. \tag{10}$$

Then the output of receive signal can be expressed as

$$\begin{aligned}\boldsymbol{x}(t)=[&\boldsymbol{a}_r(\theta_1)\otimes\boldsymbol{a}_t(r_1,\varphi_1),\boldsymbol{a}_r(\theta_2)\otimes\boldsymbol{a}_t(r_2,\varphi_2),\\ &\cdots,\boldsymbol{a}_r(\theta_P)\otimes\boldsymbol{a}_t(r_P,\varphi_P)]\boldsymbol{s}(t)+\boldsymbol{n}(t)\end{aligned} \tag{11}$$

where $\boldsymbol{s}(t)=[s_1(t),s_2(t),\cdots,s_p(t)]^{\mathrm{T}}\in\mathbb{C}^{P\times1}$ denotes a column vector that is consisting of the P targets's phases and amplitudes. $s_p(t)=\beta_p(t)e^{-j2\pi f_1r_p/c}$, and $r_p=r_{1,p}^t+r_{1,p}^r$ is the sum of the range of pth target from transmitting array and receiving array. The $NM\times1$ noise vector is $\boldsymbol{n}(t)$, which is additional white Gaussian noise vector.

According to Eq.(9), the receiver steering vector is only related to the target DOA, so we can get DOA from it independently. However, the DOD and range of the target are linearly coupled. In order to solve the DOD and range coupling problem, it is necessary to introduce subarray mode to realize the joint DOA, DOD and range estimation of bistatic FDA-MIMO radar. The transmitting array is divided into K subarrays, which are independent of each other, and the linear frequency increment between each subarray is different, so the rotation invariance is preserved. Therefore, ESPRIT method can be used to realize the decoupling of DOD and range characteristics of targets.

In the subarray mode, the transmitter steering vector of Eq.(10) can be arranged as

$$\mathbf{a}_{ts}\left(r_p,\varphi_p\right)=\begin{bmatrix}\mathbf{a}_{ts}^1\left(r_p,\varphi_p\right)\\ \mathbf{a}_{ts}^2\left(r_p,\varphi_p\right)\\ \vdots\\ \mathbf{a}_{ts}^K\left(r_p,\varphi_p\right)\end{bmatrix}. \tag{12}$$

Then we derive the transmitter steering vector for each subarray in subarray mode of FDA-MIMO radar. Let M_{ts}^k stands for the element number in the kth ($k=1,2,\cdots,K$) subarray, Δf_k represent the frequency increment of the kth subarray. In the kth subarray, the transmission frequency of mth antenna is denoted by

$$f_{ts}^{m,k}=f_{ts}^{1,k}+(m-1)\Delta f_k,m=1,2,\cdots,M_{ts}^k \tag{13}$$

where $f_{ts}^{m,k}$ represents the mth ($m=1,2,\cdots,M_{ts}^k$) antenna's transmission frequency.

Figure 3 shows the specific composition of the emission array in subarray model. In this mode, the transmit antenna frequency of each subarray increases linearly, which has the rotation invariant. In order to ensure that each subarray can provide a corresponding rotation invariant, it is necessary that the frequency increment of each subarray be different, namely $\Delta f_a\neq\Delta f_b,a\neq b$.

So the transmitter steering vector $\boldsymbol{a}_{ts}^k(r_p,\varphi_p)$ for the kth subarray is expressed as

$$\begin{aligned}\boldsymbol{a}_{ts}^k(r_p,\varphi_p)=&e^{j\frac{2\pi}{c}\left(\left(\sum_{q=1}^{k-1}M_{ts}^q\right)d_tf_1\sin(\varphi_p)+(f_1-f_{ts}^{1,k}r_p)\right)}\\ &\times\begin{bmatrix}1\\ e^{j\frac{2\pi}{c}\left(d_tf_1\sin(\varphi_p)-\Delta f_kr_p\right)}\\ \vdots\\ e^{j(M_{ts}^k-1)\frac{2\pi}{c}\left(d_tf_1\sin(\varphi_p)-\Delta f_kr_p\right)}\end{bmatrix}\end{aligned} \tag{14}$$

In fact, it is important for FDA-MIMO radar to design the frequency of subarrays, but this is not the focus of this paper. So as to facilitate the understanding of the transmitter steering vector, a non-overlapping subarray is set in this paper, and the number of antennas of each subarray should be the same, so $M_{ts}=M_{ts}^k=M/K$. The last antenna's transmission frequency of a subarray is guaranteed to be equal to the first antenna's transmission frequency of the next subarray, namely $f_{ts}^{M_{ts}^k,k}=f_{ts}^{1,k+1}$, and $f_{ts}^{1,1}=f_1$. Assume that $\Delta f_1<\Delta f_2\cdots<\Delta f_K$

In the subarray FDA-MIMO radar mode, in light of Eq.(11) and Eq.(12), the radar array mainfold matrixes of the received signal model is denoted by

$$\boldsymbol{A}=[\boldsymbol{a}_r(\theta_1)\otimes\boldsymbol{a}_{ts}(r_1,\varphi_1),\cdots,\boldsymbol{a}_r(\theta_P)\otimes\boldsymbol{a}_{ts}(r_P,\varphi_P)] \tag{15}$$

After collecting the characteristics of L snapshots, the received data is arranged as $\boldsymbol{X}=[\boldsymbol{x}(1),\boldsymbol{x}(2),\cdots,\boldsymbol{x}(L)]$, and $\boldsymbol{X}$ is written as

$$\boldsymbol{X}=\boldsymbol{A}\boldsymbol{S}^{\mathrm{T}}+\boldsymbol{N}=[\boldsymbol{A}_r\odot\boldsymbol{A}_{ts}]\boldsymbol{S}^{\mathrm{T}}+\boldsymbol{N} \tag{16}$$

where the receiving direction matrixes is $\boldsymbol{A}_r=[\boldsymbol{a}_r(\theta_1),\boldsymbol{a}_r(\theta_2),\cdots,\boldsymbol{a}_r(\theta_P)]\in\mathbb{C}^{N\times P}$, and the subarray transmitting direction matrixes can be denoted by $\boldsymbol{A}_{ts}=[\boldsymbol{a}_{ts}(r_1,\varphi_1),\boldsymbol{a}_{ts}(r_2,\varphi_2),\cdots,\boldsymbol{a}_{ts}(r_P,\varphi_P)]\in\mathbb{C}^{M\times P}$. The dimension of $\boldsymbol{X}$ is $MN\times L$, and $\boldsymbol{S}=[\boldsymbol{s}(1),\boldsymbol{s}(2),\cdots,\boldsymbol{s}(L)]^{\mathrm{T}}\in\mathbb{C}^{L\times P}$. The noise matrixes is $\boldsymbol{N}\in\mathbb{C}^{MN\times L}$.

According to the tensor unfolding in Definition 1, Eq.(16) can be seen as the slice, which follows the direction of snapshot. And we create a tensor $\boldsymbol{\mathcal{X}}\in\mathbb{C}^{M\times N\times L}$ by stacking the matrixes $\boldsymbol{X}$ along the third-dimension, and let $[\boldsymbol{\mathcal{N}}]_{(3)}^{\mathrm{T}}=\boldsymbol{N}$, we can get

$$[\boldsymbol{\mathcal{X}}]_{(3)}^{\mathrm{T}}=\boldsymbol{X}. \tag{17}$$

So we get the signal model based on tensor, which contains the multidimensional structure characteristics of signal data, so the better estimation accuracy can be obtained. In the next section, we derive the DOA, DOD and range estimation method in detail.

III. JOINT DOD, DOA AND RANGE ESTIMATION FOR BISTATIC FDA-MIMO RADAR

A. SIGNAL SUBSPACE ESTIMATION VIA HOSVD

So as to get the signal subspace that based on tensor, we adopt the HOSVD to process the tensor $\boldsymbol{\mathcal{X}} \in \mathbb{C}^{M\times N\times L}$, which is denoted by

$$\boldsymbol{\mathcal{X}} = \boldsymbol{\mathcal{G}} \times_1 \boldsymbol{U}_1 \times_2 \boldsymbol{U}_2 \times_3 \boldsymbol{U}_3 \tag{18}$$

where $\boldsymbol{\mathcal{G}} \in \mathbb{C}^{M\times N\times L}$ stands for the core tensor, $\boldsymbol{U}_1 \in \mathbb{C}^{M\times M}$, $\boldsymbol{U}_2 \in \mathbb{C}^{N\times N}$ and $\boldsymbol{U}_3 \in \mathbb{C}^{L\times L}$ are consisting of the left singular of the mode-n tensor unfolding of $\boldsymbol{\mathcal{X}}$, namely $[\boldsymbol{\mathcal{X}}]_{(n)} = \boldsymbol{U}_n\boldsymbol{\Lambda}_n\boldsymbol{V}_n^{\mathrm{H}}(n = 1, 2, 3)$, respectively. The rank of tensor $\boldsymbol{\mathcal{X}}$ is P, because it has preset P targets. Then use the truncated HOSVD of $\boldsymbol{\mathcal{X}}$, we can get the tensor based subspace that can be expressed as

$$\boldsymbol{\mathcal{X}}_s = \boldsymbol{\mathcal{G}}_s \times_1 \boldsymbol{U}_{s1} \times_2 \boldsymbol{U}_{s2} \tag{19}$$

where $\boldsymbol{U}_{sn}(n = 1, 2, 3)$ is consisting of the column vector of $\boldsymbol{U}_n$ corresponding to the first P singular values, and $\boldsymbol{\mathcal{G}} = \boldsymbol{\mathcal{X}} \times_1 \boldsymbol{U}_{s1}^{\mathrm{H}} \times_2 \boldsymbol{U}_{s2}^{\mathrm{H}} \times_3 \boldsymbol{U}_{s3}^{\mathrm{H}}$ represents the truncated core tensor.

Then using the Mode-n tensor-matrixes product in term of definition 2 and substituting $\boldsymbol{\mathcal{G}}$ into (16), we can get

$$\boldsymbol{\mathcal{X}}_s = \boldsymbol{\mathcal{X}} \times_1 (\boldsymbol{U}_{s1}\boldsymbol{U}_{s1}^{\mathrm{H}}) \times_2 (\boldsymbol{U}_{s2}\boldsymbol{U}_{s2}^{\mathrm{H}}) \times_3 \boldsymbol{U}_{s3}^{\mathrm{H}} \tag{20}$$

According to definition 1, the tensor $\boldsymbol{\mathcal{X}}_s$ is unfolding in mode-3, and then combined with the definition 3 of the properties of the mode product, we can get the tensor based signal subspace, which can be expressed as

$$\boldsymbol{U}_s = [\boldsymbol{\mathcal{X}}_s]_{(3)}^{\mathrm{T}} = (\boldsymbol{U}_{s2}\boldsymbol{U}_{s2}^{\mathrm{H}} \otimes \boldsymbol{U}_{s1}\boldsymbol{U}_{s1}^{\mathrm{H}})[\boldsymbol{\mathcal{X}}]_{(3)}^{\mathrm{T}}\boldsymbol{U}_{s3}^{*} \tag{21}$$

where $[\boldsymbol{\mathcal{X}}]_{(3)} = \boldsymbol{U}_3\boldsymbol{\Lambda}_3\boldsymbol{V}_3^{\mathrm{H}}$. Therefor, the singular value decomposition of $[\boldsymbol{\mathcal{X}}]_{(3)}^{\mathrm{T}}$ can be denoted by $[\boldsymbol{\mathcal{X}}]_{(3)}^{\mathrm{T}} \approx \boldsymbol{V}_{s3}^{*}\boldsymbol{\Lambda}_{s3}\boldsymbol{U}_{s3}^{\mathrm{T}}$, and then $[\boldsymbol{\mathcal{X}}]_{(3)}^{\mathrm{T}}$ can be substituted into Eq.(21), the simplification result can be expressed as

$$\boldsymbol{U}_s = (\boldsymbol{U}_{s2}\boldsymbol{U}_{s2}^{\mathrm{H}} \otimes \boldsymbol{U}_{s1}\boldsymbol{U}_{s1}^{\mathrm{H}})\boldsymbol{V}_{s3}^{*}\boldsymbol{\Lambda}_{s3} \tag{22}$$

So the tensor based signal subspace $\boldsymbol{U}_s$ has been estimated.

B. DOA ESTIMATION

According to the rotational invariance of the signal subspace, the selection matrixess needs to be defined in order to obtain DOA, which as follows

$$\begin{cases} \boldsymbol{Q}_{r1} = [\,\boldsymbol{I}_{(N-1)}\ \boldsymbol{0}_{(N-1)\times 1}\,] \otimes \boldsymbol{I}_M \\ \boldsymbol{Q}_{r2} = [\,\boldsymbol{0}_{(N-1)\times 1}\ \boldsymbol{I}_{(N-1)}\,] \otimes \boldsymbol{I}_M \end{cases} \tag{23}$$

Then using the rotation invariance of the subarray, the $\boldsymbol{U}_s$ is divided into two parts, which can is written by

$$\begin{cases} \boldsymbol{U}_{r1} = \boldsymbol{Q}_{r1}\boldsymbol{U}_s \\ \boldsymbol{U}_{r2} = \boldsymbol{Q}_{r2}\boldsymbol{U}_s \end{cases} \tag{24}$$

Eigenvalue decomposition is performed, we can get

$$\begin{bmatrix} \boldsymbol{U}_{r1}^{\mathrm{H}} \\ \boldsymbol{U}_{r2}^{\mathrm{H}} \end{bmatrix} [\,\boldsymbol{U}_{r1}\ \boldsymbol{U}_{r2}\,] = \boldsymbol{E}_r\boldsymbol{\Lambda}_r\boldsymbol{E}_r^{\mathrm{H}} \tag{25}$$

And divide $\boldsymbol{E}_r \in \mathbb{C}^{K\times K}$ into four sub matrices, which can be denoted by

$$\boldsymbol{E}_r = \begin{bmatrix} \boldsymbol{E}_{r11}\ \boldsymbol{E}_{r12} \\ \boldsymbol{E}_{r21}\ \boldsymbol{E}_{r22} \end{bmatrix} \tag{26}$$

where the dimensions of $\boldsymbol{E}_{r11}$, $\boldsymbol{E}_{r12}$, $\boldsymbol{E}_{r21}$ and $\boldsymbol{E}_{r22}$ are all $K \times K$.

So we can get the matrixes $\boldsymbol{\Psi}_r$ contain DOA information of targets and perform eigenvalue decomposition, which can be expressed as

$$\boldsymbol{\Psi}_r = -\boldsymbol{E}_{r12}\boldsymbol{E}_{r22}^{-1} = \boldsymbol{T}\boldsymbol{\Phi}_r\boldsymbol{T}^{-1} \tag{27}$$

where $\boldsymbol{\Phi}_r$ is a diagonal matrixes. It can be expressed as

$$\boldsymbol{\Phi}_r = diag\begin{bmatrix} e^{j2\pi d_r f_1 \sin\theta_1/c} \\ e^{j2\pi d_r f_2 \sin\theta_2/c} \\ \vdots \\ e^{j2\pi d_r f_p \sin\theta_p/c} \end{bmatrix} \tag{28}$$

The DOA $\hat{\theta}_p$ of the pth target can be get by

$$\hat{\theta}_p = arcsin\left(\frac{angle(\boldsymbol{\phi}_r^p)c}{2\pi d_r f_1}\right)\frac{180^\circ}{\pi} \tag{29}$$

where $\boldsymbol{\phi}_r^p$ represents the pth element of $\boldsymbol{\Phi}_r$.

C. DOD AND RANGE ESTIMATION

In subarray FDA-MIMO radar mode, each subarray and receiving array can be regarded as a whole, which contains corresponding signal subspace. Therefore, we define the selection matrixes to select out the signal subspace of each subarray.

$$\boldsymbol{Q}_s^k = \boldsymbol{I}_N \otimes \left[\,\boldsymbol{0}_{[\,(k-1)M_{ts}\,]}\ \boldsymbol{I}_{M_{ts}}\ \boldsymbol{0}_{[\,M_{ts}\times(M-kM_{ts})\,]}\,\right] \tag{30}$$

where $\boldsymbol{Q}_s^k \in \mathbb{C}^{M_{ts}N\times MN}$ represents the selection matrixes for the kth subarray. Then the signal subspace $\boldsymbol{U}_s^k$ of each subarray can be expressed as

$$\boldsymbol{U}_s^k = \boldsymbol{Q}_s^k\boldsymbol{U}_s \tag{31}$$

Then we define the selection matrixes to get the DOD and range information of targets from each subarray, which can be written by

$$\begin{cases} \boldsymbol{Q}_{t1} = \boldsymbol{I}_N \otimes \begin{bmatrix} \boldsymbol{I}_{(M_{ts}-1)}\ \boldsymbol{0}_{(M_{ts}-1)\times 1} \\ \boldsymbol{0}_{(M_{ts}-1)\times 1}\ \boldsymbol{I}_{(M_{ts}-1)} \end{bmatrix} \\ \boldsymbol{Q}_{t2} = \boldsymbol{I}_N \otimes \begin{bmatrix} \boldsymbol{I}_{(M_{ts}-1)}\ \boldsymbol{0}_{(M_{ts}-1)\times 1} \\ \boldsymbol{0}_{(M_{ts}-1)\times 1}\ \boldsymbol{I}_{(M_{ts}-1)} \end{bmatrix} \end{cases} \tag{32}$$

We can decompose $\boldsymbol{U}_{ts}^k$ into two parts,

$$\begin{cases} \boldsymbol{U}_{t1}^k = \boldsymbol{Q}_{t1}\boldsymbol{U}_s^k \\ \boldsymbol{U}_{t2}^k = \boldsymbol{Q}_{t2}\boldsymbol{U}_s^k \end{cases} \tag{33}$$

Similarly, the Eq.(25)-(27) in Section(III-B) can be employed to get $\boldsymbol{\Psi}_t^k$, which contains target's DOD and range information in the kth subarray. Because of the rotation invariance, $\boldsymbol{\Psi}_r$ and $\boldsymbol{\Psi}_t^k$ span the same subspace. So we match the DOA with DOD and range of the target, and diagonalize

the $\boldsymbol{\Psi}_t^k$ use the matrix $\boldsymbol{T}$, which is composed of eigenvectors of $\boldsymbol{\Psi}_r$ in (27). It can be written by

$$\boldsymbol{\Phi}_t^k = \boldsymbol{T}^{-1}\boldsymbol{\Psi}_t^k\boldsymbol{T} \tag{34}$$

And the specific composition of $\boldsymbol{\Phi}_t^k$ as follows:

$$\boldsymbol{\Phi}_t^k = diag\begin{bmatrix} e^{j\frac{2\pi}{c}[d_r f_1 \sin\varphi_1 - \Delta f_1 r_1]} \\ e^{j\frac{2\pi}{c}[d_r f_1 \sin\varphi_1 - \Delta f_2 r_2]} \\ \vdots \\ e^{j\frac{2\pi}{c}[d_r f_1 \sin\varphi_1 - \Delta f_K r_p]} \end{bmatrix} \tag{35}$$

The DOD and range information can be obtained by extracting the phase of $\boldsymbol{\Phi}_t^k$:

$$\begin{cases} \frac{2\pi}{c} d_t f_1 \sin(\varphi_p) - \frac{2\pi}{c}\Delta f_1 r_p = angle(\boldsymbol{\phi}_{ts}^{p,1}) - 2k_1\pi \\ \frac{2\pi}{c} d_t f_1 \sin(\varphi_p) - \frac{2\pi}{c}\Delta f_2 r_p = angle(\boldsymbol{\phi}_{ts}^{p,2}) - 2k_2\pi \\ \vdots \\ \frac{2\pi}{c} d_t f_1 \sin(\varphi_p) - \frac{2\pi}{c}\Delta f_K r_p = angle(\boldsymbol{\phi}_{ts}^{p,K}) - 2k_K\pi \end{cases} \tag{36}$$

where $\boldsymbol{\phi}_{ts}^{p,k}$ contains the phase information of pth target in kth subarray, and $k_i \in \mathbb{Z}, i = 1, 2, \cdots, K$. It is unable to determine k_K due to the existence of $angle(\boldsymbol{\phi}_{ts}^{p,k})$ phase period fuzzy problem. $\Delta f_1 < \Delta f_2 < \cdots < \Delta f_K$ has been preset in Section(II-B), let each equation subtract the latter equation in Eq.(36). If simplify the result, we can get as follows:

$$\begin{cases} \frac{\Delta f_2 - \Delta f_1}{c} r_p = \frac{angle(\boldsymbol{\phi}_{ts}^{p,1}/\boldsymbol{\phi}_{ts}^{p,2})}{2\pi} + (k_2 - k_1) \\ \frac{\Delta f_3 - \Delta f_2}{c} r_p = \frac{angle(\boldsymbol{\phi}_{ts}^{p,2}/\boldsymbol{\phi}_{ts}^{p,3})}{2\pi} + (k_3 - k_2) \\ \vdots \\ \frac{\Delta f_K - \Delta f_{K-1}}{c} r_p = \frac{angle(\boldsymbol{\phi}_{ts}^{p,K-1}/\boldsymbol{\phi}_{ts}^{p,K})}{2\pi} \\ +(k_K - k_{K-1}) \end{cases} \tag{37}$$

For the convenience of subsequent analysis and calculation, the Eq.(37) can be sorted out

$$\boldsymbol{h}_p = \begin{bmatrix} h_{p,1} \\ h_{p,2} \\ \vdots \\ h_{p,K-1} \end{bmatrix} = \begin{bmatrix} \frac{\Delta f_2 - \Delta f_1}{c} \\ \frac{\Delta f_3 - \Delta f_2}{c} \\ \vdots \\ \frac{\Delta f_K - \Delta f_{K-1}}{c} \end{bmatrix} \tag{38}$$

and similarly $\boldsymbol{\zeta}_p = [\zeta_{p,1}, \zeta_{p,2}, \cdots, \zeta_{p,K-1}]^{\mathrm{T}}$, where the ith element is

$$\begin{aligned} \zeta_{p,i} &= angle(\boldsymbol{\phi}_{ts}^{p,i}/\boldsymbol{\phi}_{ts}^{p,i+1}) + (k_{i+1} - k_i) \\ &= angle(\boldsymbol{\phi}_{ts}^{p,i}) - angle(\boldsymbol{\phi}_{ts}^{p,i+1}) + (k_{i+1} - k_i) \end{aligned} \tag{39}$$

In this case, the (37) can be summarized as:

$$\begin{cases} h_{p,1}* & r_p = \zeta_{p,1} \\ h_{p,2}* & r_p = \zeta_{p,2} \\ & \vdots \\ h_{p,K-1}* & r_p = \zeta_{p,K-1} \end{cases} \Rightarrow \boldsymbol{h}_p r_p = \boldsymbol{\zeta}_p \tag{40}$$

The general form of (40) can be expressed as

$$\begin{aligned} &2\pi \frac{\Delta f_{ts}^{i+1} - \Delta f_{ts}^{i}}{c} r_p \\ &\quad = angle(\boldsymbol{\phi}_{ts}^{p,i}) - angle(\boldsymbol{\phi}_{ts}^{p,i+1}) + 2\pi(k_{i+1} - k_i) \end{aligned} \tag{41}$$

As can be seen from Eq.(41) that in order to determine the range parameter, it is necessary to ensure:

$$0 < 2\pi \frac{\Delta f_{ts}^{i+1} - \Delta f_{ts}^{i}}{c} r_p \leqslant 2\pi \tag{42}$$

where $2\pi \frac{\Delta f_{ts}^{i+1} - \Delta f_{ts}^{i}}{c} r_p > 0$ is obvious, which is because the range r_p must be positive and $\Delta f_{ts}^1 < \Delta f_{ts}^2 \cdots < \Delta f_{ts}^K$. The $2\pi \frac{\Delta f_{ts}^{i+1} - \Delta f_{ts}^{i}}{c} r_p \leqslant 2\pi$ guarantees that the $(k_{i+1} - k_i)$ can be uniquely determined in this case. So we can figure out the value of $(k_{i+1} - k_i)$ can be written by

$$k_{i+1} - k_i = \begin{cases} 1, & angle(\boldsymbol{\phi}_{ts}^{p,i}) < angle(\boldsymbol{\phi}_{ts}^{p,i+1}) \\ 0, & angle(\boldsymbol{\phi}_{ts}^{p,i}) > angle(\boldsymbol{\phi}_{ts}^{p,i+1}) \end{cases} \tag{43}$$

It is clear from (42) that the value range of r_p is given by

$$r_p \leqslant \frac{c}{\Delta f_{ts}^{i+1} - \Delta f_{ts}^{i}} \tag{44}$$

Then combined with all the equations in (40), the (44) can be arranged as

$$r_p \leqslant \frac{c}{max(\Delta f_{ts}^{i+1} - \Delta f_{ts}^{i})} \tag{45}$$

where we can get the $i = 1, 2, \cdots, K-1$.

Therefore, the detection range of target should be considered in the actual radar configuration, which is to meet the Eq.(45).

We can solve $angle(\boldsymbol{\phi}_{ts}^{p,i})$ from Eq.(35) and substitute $(k_{i+1} - k_i)$ of Eq.(43) into Eq.(40). Using the least square method, so we can estimated the range r_p of target, which is expressed as

$$\hat{r}_p = \boldsymbol{h}_p^{\dagger}\boldsymbol{\zeta}_p \tag{46}$$

where the $\hat{r}_p$ represents the estimated range of the pth target.

Then substitute $\hat{r}_p$ into Eq.(36) can be expressed as

$$\begin{cases} \frac{2\pi}{c} d_t f_1 \sin(\varphi_p) = angle(\boldsymbol{\phi}_{ts}^{p,1}) - 2k_1\pi + \frac{2\pi}{c}\Delta f_{ts}^1 r_p \\ \frac{2\pi}{c} d_t f_1 \sin(\varphi_p) = angle(\boldsymbol{\phi}_{ts}^{p,2}) - 2k_2\pi + \frac{2\pi}{c}\Delta f_{ts}^2 r_p \\ \vdots \\ \frac{2\pi}{c} d_t f_1 \sin(\varphi_p) = angle(\boldsymbol{\phi}_{ts}^{p,K}) - 2k_K\pi + \frac{2\pi}{c}\Delta f_{ts}^K r_p \end{cases} \tag{47}$$

In fact, the $2d_t f_1/c \leqslant 1$ due to the transmmitting array spacing setting. After a series of calculations, we can determine $k_i(i = 1, 2, \cdots, K)$ by

$$k_i = \left\lfloor \frac{angle(\boldsymbol{\phi}_{ts}^{p,i}) + \frac{2\pi}{c}\Delta f_{ts}^{i}\hat{r}_p + \pi}{2\pi} \right\rfloor, \ i=1, 2, \cdots, K \quad (48)$$

Then the k_i can be substituted into Eq.(47), and the DOD $\hat{\varphi}_p$ of the pth target can be obtained by least square method:

$$\hat{\varphi}_p = arcsin\left(\frac{(angle(\boldsymbol{\phi}_{ts}^{p,i}) - 2k_i\pi + \frac{2\pi}{c}\Delta f_{ts}^{i} r_p)c}{2\pi d_t f_1} \right) \frac{180^\circ}{\pi} \quad (49)$$

So we can estimate the DOA $\hat{\theta}$, DOD $\hat{\varphi}$ and range $\hat{r}$ of target by the proposed method.

IV. PERFORMANCE ANALYSIS

A. COMPUTATIONAL COMPLEXITY

So as to better analyze the performance of the method, we calculated the computational complexity of the proposed method. The specific derivation of each part is as follows:
(1)Hosvd of the tensor based received signal $\boldsymbol{\mathcal{X}} \in \mathbb{C}^{M\times N\times L}$ in Eq.(18) requires $O(\,MNL(M+N+L)\,)$;
(2)Computing the signal subspace $\boldsymbol{U}_s$ in Eq.(22) is $O(\,4MNLP\,)$;
(3)Obtaining the contain DOA information matrix $\boldsymbol{\Psi}_r$ is $O(\,M(N-1)(2MNP+4P^2)+P^3\,)$;
(4)The eigenvalue decomposition of $\boldsymbol{\Psi}_r$ is $O(P^3)$;
(5)Similarly, obtaining the contain DOD and range information matrix $\boldsymbol{\Psi}_t^k$ is $O(\sum_{i=1}^{K}(N(M_{ts}-1)(2M_{ts}NP+4P^2)+P^3))$;
(6)The match DOD and range with DOA in Eq.(34) is $O(KP^3)$;
and the process of solving phase period fuzzy problem is relatively simple, whose computational complexity can be ignored.

In summary, the proposed method's computational complexity can be summarized as $O(MNL(M+N+L)+4MNLP+2(K+1)P^3+(2MN-M-N)(2MNP+4MNP^2))$.

B. ADVANTAGE ANALYSIS FOR TENSOR-BASED

The tensor used to build the signal model is the main difference, which between the proposed method and the traditional subspace method. It gets the multi-dimensional structural characteristics of data, thereby improving the estimation accuracy of the signal subspace. The largest angle (LA) is the standard for evaluating the accuracy, which between the estimation subspace and the real subspace. The criterion for evaluating the accuracy is the largest angle (LA), which between the estimation subspace and the real subspace. It is shown as follows:

$$LA = \cos^{-1}\left(\delta_{min}\left[orth(\boldsymbol{A}^{\mathrm{H}})orth(\boldsymbol{U}_s^{\mathrm{H}})\right]\right) \quad (50)$$

where $orth(\cdot)$ represents the orthogonal basis, and $\delta_{min}(\cdot)$ is the smallest singular value.

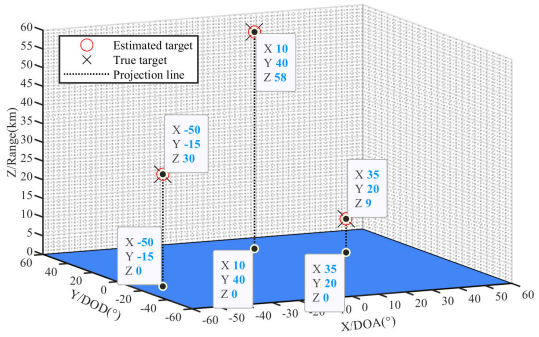

FIGURE 4. 3D point cloud of estimated targets.

V. NUMERICAL SIMULATIONS

In this section, the several simulation experiments are used to verify the superiority of the proposed method. Unless otherwise specified, the bistatic FDA-MIMO radar's transmitting array and receiving array are ULA in this paper, and the total of antennas of their is equal. In the simulation, we set the transmission frequency of the first transmitting antenna is $f_1 = 10GHz$. The antenna spacing is preser $d_t = d_r = \frac{c}{2f_{max}}$, with f_{max} is the largest transmission frequency. Moreover, the simulation results are obtained by $T = 500$ Monte Carlo trials.

A. 3D POINT CLOUD OF TARGET PARAMETERS

In this simulation, we preset the number of transmitting antennas is $M = 18$, and the number of receiving antennas is $N = 18$. Then decompose the transmitting array into $K = 3$ subarrays, where each of subarray has $M_{ts} = 6$ transmitting antennas. The transmission frequency increment of each subarray is $\Delta f_1 = 5000Hz$, $\Delta f_2 = 10000Hz$ and $\Delta f_3 = 15000Hz$, respectively. Note that the number of snapshots is $L = 300$ and $SNR = 20dB$. A several unrelated targets with the DOA, DOD and range are located at $(\theta_1, \varphi_1, r_1) = (-50^\circ, -15^\circ, 30km)$, $(\theta_2, \varphi_2, r_2) = (10^\circ, 40^\circ, 58km)$ and $(\theta_3, \varphi_3, r_3) = (35^\circ, 20^\circ, 9km)$, respectively.

Figure 4 shows the location of the estimated targets in $SNR = 20dB$ and $L = 300$. The X-axis, Y-axis and Z-axis represent DOA, DOD and range, respectively. It is manifest from the figure 4 that the estimated targets landing points are very concentrated and identical to the locations of the real targets. This can prove the stability and accuracy of the proposed method are excellent.

B. SUBSPACE ESTIMATION ACCURACY

For the proposed method, the main evaluation criterion is the root mean square error (RMSE) performance, which is determined by the subspace estimation accuracy. In term of the section(IV-B), we simulate the subspace accuracy versus SNR and the number of snapshots, which are displayed in figure 5 and figure 6, respectively. We take $L = 50$ for figure 5 and $SNR = 5dB$ for figure 6. Radar structure and target parameters are consistent with above.

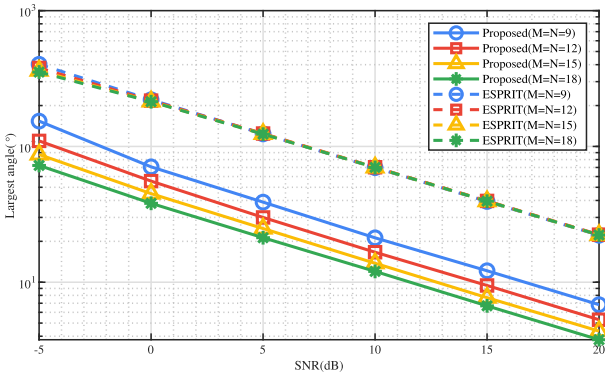

FIGURE 5. Subspace accuracy varies with SNR.

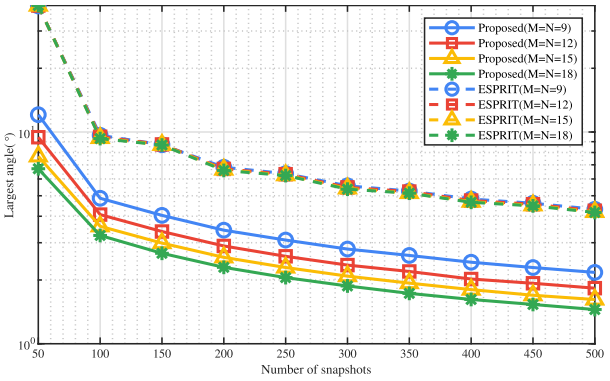

FIGURE 6. Subspace accuracy varies with number of snapshots.

Figure 5 shows the estimated subspace's accuracy, with the number of antennas being $M = N = 9, 12, 15, and 18$. It is manifest from figure 5 that the performance of methods can be raised when the increase of SNR and the number of snapshots. And in the same case, the performance of the proposed method is more outstanding than the ESPRIT method. Meanwhile, with the increase in the number of antennas, these method's performance can be gradually raised. However, compared with the proposed method, the total of antennas has a weak effect on the ESPRIT method's performance. The reason is that the proposed method utilizes tensor to save the structure characteristics of FDA-MIMO radar array antennas. Therefore, with the increase in the number of antennas, the performance of the proposed method based on tensor is much higher than the method based on matrix decomposition.

C. RMSE PERFORMANCE

To measure the performance of the method, we defined the RMSE of estimation parameters (DOA, DOD and range) as follows:

$$\mathrm{RMSE}_{\theta} = \frac{1}{P}\sum_{p=1}^{P}\sqrt{\frac{1}{T}\sum_{t=1}^{T}\left(\hat{\theta}_p^t - \theta_p\right)^2} \tag{51}$$

$$\mathrm{RMSE}_{\varphi} = \frac{1}{P}\sum_{p=1}^{P}\sqrt{\frac{1}{T}\sum_{t=1}^{T}\left(\hat{\varphi}_p^t - \varphi_p\right)^2} \tag{52}$$

$$\mathrm{RMSE}_{r} = \frac{1}{P}\sum_{p=1}^{P}\sqrt{\frac{1}{T}\sum_{t=1}^{T}\left(\hat{r}_p^t - r_p\right)^2} \tag{53}$$

where $\hat{\theta}_p^t$, $\hat{\varphi}_p^t$ and $\hat{r}_p^t$ represent the estimated results of the DOA, DOD and range of the pth target in the tth Monte Carlo trials, respectively. We introduce the ESPRIT method as the comparison method to analyze RMSE performance.

Figure 7 and figure 8 show the change of the Angle and range RMSE of these methods with SNR in $L = 50$, respectively. In addition, CRB has been introduced as the performance standard of the method. It can be seen from figure 7 and figure 8 that the performance of the proposed method is more outstanding than the ESPRIT

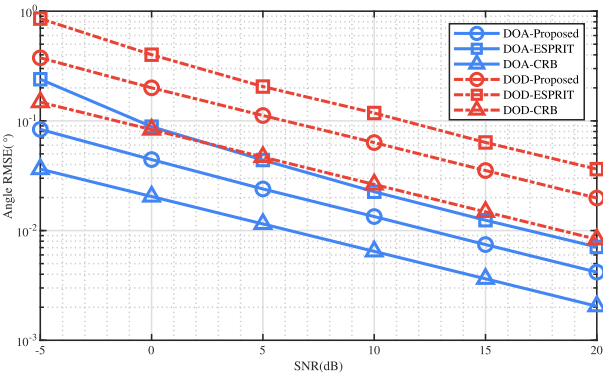

FIGURE 7. Angle RMSE versus SNR.

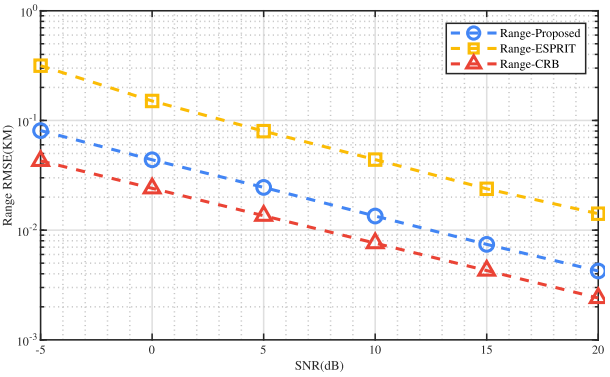

FIGURE 8. Range RMSE versus SNR.

method. Meanwhile, the proposed method has higher performance under the same SNR and the number of snapshots, because the proposed method adopts tensor, which can make the most of the multidimensional structure characteristics inherent in the received signal. Besides, it is noticed from Figure 7 that the estimation accuracy of DOD is worse than DOA's. The reason is that the range error is substituted into the DOD estimation, which leads to the decline of the estimation accuracy of DOD. The fundamental reason is the structure of FDA radar, because the transmitter steering vector contains both DOD and range information, and only part of its information is used in the DOD and range estimation.

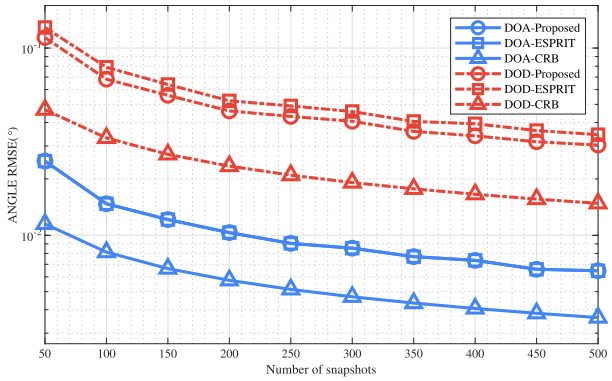

FIGURE 9. Angle RMSE versus the number of snapshots.

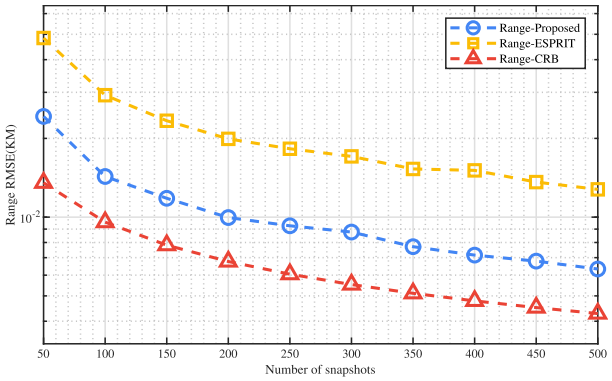

FIGURE 10. Range RMSE versus the number of snapshots.

Figure 9 and figure 10 compare the performance of the methods with the number of snapshots in $SNR = 5dB$. Similarly, we introduce CRB to measure the method's performance. It can be found that the RMSE of these methods decreases with the increase of the number of snapshots, which indicates that the performance of these methods is constantly improving and is gradually close to parallel with the trend of CRB. Moreover, the curve of the method is close to the trend of CRB when the number of snapshots increases to large enough, which indicates that these method's performance gradually tends to be stable.

D. PROBABILITY OF SUCCESSFUL DETECTION

The probability of successful detection (PSD) is another important criterion for measuring method's performance. The success of the estimation can be determined by setting the fluctuation range, which can be expressed as:

$$\text{PSD} = \frac{V}{T} \times 100\% \tag{54}$$

where the number of successful estimates is V. In this simulation, it is considered as a successful estimate when the absolute error between the actual value and the estimated value of angle and range is less than $0.1°$ and $0.1km$.

Figure 11 shows the change of PSD versus SNR of the proposed method in $L = 50$. It is manifest from figure 11 that

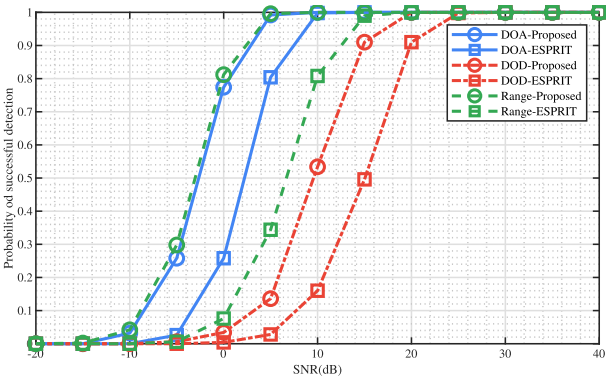

FIGURE 11. Probability of successful detection versus SNR.

both the proposed method and the ESPRIT method achieve 100% successful detection in the high SNR region, which is usually referred to as the SNR threshold. And the proposed method has a low threshold. Moreover, the SNR thresholds of DOA and range are lower than DOD's, which is similar to figure 7. Because DOA and range are estimated independently, the range needs to be substituted in the process of estimate DOD, so the range's error will be introduced, and DOD's estimation accuracy will be reduced. The accuracy of the proposed method can be directly proved by the PSD.

VI. CONCLUSION

In this paper, we considers an edge computing enabling IoT systemn for vehicle location with bistatic FDA-MIMO radar, and then propose a tensor-based subspace method for joint DOA, DOD, and range estimation. A tensor signal model is constructed to capture the multidimensional structure characteristics of the received data, and the accuracy and stability of the parameter estimation are improved. Firstly, so as to solve the coupling of parameters DOD and range, the transmitting array is constructed by subarrays, which is with different frequency increments. Then the phase ambiguity is solved by controlling the target range parameter and a parameter matching method is proposed. The proposed method can obtain higher parameter estimation accuracy at low SNR and has good compatibility in the small array and many targets scenarios. Numerical simulations have shown the superiority of the method. We will further improve the performance of the method and apply it to more application scenarios in the future.

REFERENCES

[1] L. Sun, L. Wan, and X. Wang, "Learning-based resource allocation strategy for industrial IoT in UAV-enabled MEC systems," *IEEE Trans. Ind. Informat.*, early access, Sep. 15, 2020, doi: 10.1109/TII.2020.3024170.
[2] H. Liao, Z. Zhou, W. Kong, Y. Chen, X. Wang, Z. Wang, and S. Al Otaibi, "Learning-based intent-aware task offloading for air-ground integrated vehicular edge computing," *IEEE Trans. Intell. Transport. Syst.*, early access, Oct. 29, 2020, doi: 10.1109/TITS.2020.3027437.
[3] D. Zhang, Z. Zhou, C. Xu, Y. Zhang, J. Rodriguez, and T. Sato, "Capacity analysis of NOMA with mmWave massive MIMO systems," *IEEE J. Sel. Areas Commun.*, vol. 35, no. 7, pp. 1606–1618, Jul. 2017, doi: 10.1109/JSAC.2017.2699059.

[4] L. Wan, L. Sun, X. Kong, Y. Yuan, K. Sun, and F. Xia, "Task-driven resource assignment in mobile edge computing exploiting evolutionary computation," *IEEE Wireless Commun.*, vol. 26, no. 6, pp. 94–101, Dec. 2019.

[5] H. Krim and M. Viberg, "Two decades of array signal processing research: The parametric approach," *IEEE Signal Process. Mag.*, vol. 13, no. 4, pp. 67–94, Jul. 1996.

[6] E. Fishler, A. Haimovich, R. Blum, L. Cimini, D. Chizhik, and R. Valenzuela, "Performance of MIMO radar systems: Advantages of angular diversity," in *Proc. Conf. Rec. 38th Asilomar Conf. Signals, Syst. Comput.*, vol. 1, 2004, pp. 305–309.

[7] X. Wang, L. Wan, M. Huang, C. Shen, Z. Han, and T. Zhu, "Low-complexity channel estimation for circular and noncircular signals in virtual MIMO vehicle communication systems," *IEEE Trans. Veh. Technol.*, vol. 69, no. 4, pp. 3916–3928, Apr. 2020.

[8] H. Wang, L. Wan, M. Dong, K. Ota, and X. Wang, "Assistant vehicle localization based on three collaborative base stations via SBL-based robust DOA estimation," *IEEE Internet Things J.*, vol. 6, no. 3, pp. 5766–5777, Jun. 2019.

[9] X. Wang, M. Huang, and L. Wan, "Joint 2D-DOD and 2D-DOA estimation for coprime EMVS–MIMO radar," *Circuits, Syst., Signal Process.*, Jan. 2021, doi: 10.1007/s00034-020-01605-5.

[10] E. Fishler, A. Haimovich, R. Blum, D. Chizhik, L. Cimini, and R. Valenzuela, "MIMO radar: An idea whose time has come," in *Proc. IEEE Radar Conf.*, Apr. 2004, pp. 71–78.

[11] L. Wan, L. Sun, K. Liu, X. Wang, Q. Lin, and T. Zhu, "Autonomous vehicle source enumeration exploiting non-cooperative UAV in software defined Internet of vehicles," *IEEE Trans. Intell. Transport. Syst.*, early access, Sep. 23, 2020, doi: 10.1109/TITS.2020.3018377.

[12] P. V. Amadori and C. Masouros, "Low RF-complexity millimeter-wave beamspace-MIMO systems by beam selection," *IEEE Trans. Commun.*, vol. 63, no. 6, pp. 2212–2223, Jun. 2015.

[13] P. Antonik, M. C. Wicks, H. D. Griffiths, and C. J. Baker, "Range-dependent beamforming using element level waveform diversity," in *Proc. Int. Waveform Diversity Design Conf.*, Jan. 2006, pp. 1–6.

[14] P. Antonik, M. C. Wicks, H. D. Griffiths, and C. J. Baker, "Frequency diverse array radars," in *Proc. IEEE Conf. Radar*, Apr. 2006, p. 3.

[15] Q. Liu, J. Xu, Z. Ding, and H. C. So, "Target localization with jammer removal using frequency diverse array," *IEEE Trans. Veh. Technol.*, vol. 69, no. 10, pp. 11685–11696, Oct. 2020.

[16] W.-Q. Wang, H. C. So, and A. Farina, "An overview on time/frequency modulated array processing," *IEEE J. Sel. Topics Signal Process.*, vol. 11, no. 2, pp. 228–246, Mar. 2017.

[17] S. Qin, Y. D. Zhang, M. G. Amin, and F. Gini, "Frequency diverse coprime arrays with coprime frequency offsets for multitarget localization," *IEEE J. Sel. Topics Signal Process.*, vol. 11, no. 2, pp. 321–335, Mar. 2017.

[18] Y. Liu, H. Ruan, L. Wang, and A. Nehorai, "The random frequency diverse array: A new antenna structure for uncoupled direction-range indication in active sensing," *IEEE J. Sel. Topics Signal Process.*, vol. 11, no. 2, pp. 295–308, Mar. 2017.

[19] J. Xiong, W.-Q. Wang, and K. Gao, "FDA-MIMO radar Range–Angle estimation: CRLB, MSE, and resolution analysis," *IEEE Trans. Aerosp. Electron. Syst.*, vol. 54, no. 1, pp. 284–294, Feb. 2018.

[20] W.-Q. Wang and H. Shao, "Range-angle localization of targets by a double-pulse frequency diverse array radar," *IEEE J. Sel. Topics Signal Process.*, vol. 8, no. 1, pp. 106–114, Feb. 2014.

[21] W.-Q. Wang, "Subarray-based frequency diverse array radar for target range-angle estimation," *IEEE Trans. Aerosp. Electron. Syst.*, vol. 50, no. 4, pp. 3057–3067, Oct. 2014.

[22] T. Xu, Y. Yang, M. Huang, H. Wang, D. Wu, and Q. Yi, "Tensor-based angle and range estimation method in monostatic FDA-MIMO radar," *Math. Problems Eng.*, vol. 2020, pp. 1–8, Aug. 2020.

[23] D. Wipf and S. Nagarajan, "Beamforming using the relevance vector machine," in *Proc. 24th Int. Conf. Mach. Learn. (ICML)*, 2007, pp. 1023–1030.

[24] W.-Q. Wang and H. C. So, "Transmit subaperturing for range and angle estimation in frequency diverse array radar," *IEEE Trans. Signal Process.*, vol. 62, no. 8, pp. 2000–2011, Apr. 2014.

[25] K. Gao, H. Shao, H. Chen, J. Cai, and W.-Q. Wang, "Impact of frequency increment errors on frequency diverse array MIMO in adaptive beamforming and target localization," *Digit. Signal Process.*, vol. 44, pp. 58–67, Sep. 2015.

[26] J. Xu, G. Liao, S. Zhu, L. Huang, and H. C. So, "Joint range and angle estimation using MIMO radar with frequency diverse array," *IEEE Trans. Signal Process.*, vol. 63, no. 13, pp. 3396–3410, Jul. 2015.

[27] X. Zhang, L. Xu, L. Xu, and D. Xu, "Direction of departure (DOD) and direction of arrival (DOA) estimation in MIMO radar with reduced-dimension MUSIC," *IEEE Commun. Lett.*, vol. 14, no. 12, pp. 1161–1163, Dec. 2010.

[28] X. Wang, Y. Zhu, M. Huang, J. Wang, L. Wan, and G. Bi, "Unitary matrix completion-based DOA estimation of noncircular signals in nonuniform noise," *IEEE Access*, vol. 7, pp. 73719–73728, 2019.

[29] D. Meng, X. Wang, M. Huang, L. Wan, and B. Zhang, "Robust weighted subspace fitting for DOA estimation via block sparse recovery," *IEEE Commun. Lett.*, vol. 24, no. 3, pp. 563–567, Mar. 2020.

[30] D. Nion and N. D. Sidiropoulos, "Tensor algebra and multidimensional harmonic retrieval in signal processing for MIMO radar," *IEEE Trans. Signal Process.*, vol. 58, no. 11, pp. 5693–5705, Nov. 2010.

[31] Y.-Q. Yang, H. Wang, H.-Q. Wang, S.-Q. Gu, D.-L. Xu, and S.-L. Quan, "Optimization of sparse frequency diverse array with time-invariant spatial-focusing beampattern," *IEEE Antennas Wireless Propag. Lett.*, vol. 17, no. 2, pp. 351–354, Feb. 2018.

[32] W. Khan and I. M. Qureshi, "Frequency diverse array radar with time-dependent frequency offset," *IEEE Antennas Wireless Propag. Lett.*, vol. 13, pp. 758–761, 2014.

[33] L. Wan, Y. Sun, L. Sun, Z. Ning, and J. J. P. C. Rodrigues, "Deep learning based autonomous vehicle super resolution DOA estimation for safety driving," *IEEE Trans. Intell. Transp. Syst.*, early access, Aug. 21, 2020, doi: .10.1109/TITS.2020.3009223

[34] X. Wang, W. Wang, J. Liu, Q. Liu, and B. Wang, "Tensor-based real-valued subspace approach for angle estimation in bistatic MIMO radar with unknown mutual coupling," *Signal Process.*, vol. 116, pp. 152–158, Nov. 2015.

[35] C. Palmer, "Music performance: Movement and coordination," in *The Psychology of Music*, 3rd ed., D. Deutsch, Ed. New York, NY, USA: Academic, 2013, ch. 10, pp. 405–422.

[36] Q. Liu, W. Wang, D. Liang, and X. Wang, "Real-valued reweighted ℓ_1 norm minimization method based on data reconstruction in MIMO radar," *IEICE Trans. Commun.*, vol. E98.B, no. 11, pp. 2307–2313, 2015.

[37] Q. Liu, H. C. So, and Y. Gu, "Off-grid DOA estimation with nonconvex regularization via joint sparse representation," *Signal Process.*, vol. 140, pp. 171–176, Nov. 2017.

[38] D. Malioutov, M. Cetin, and A. S. Willsky, "A sparse signal reconstruction perspective for source localization with sensor arrays," *IEEE Trans. Signal Process.*, vol. 53, no. 8, pp. 3010–3022, Aug. 2005.

[39] P. Gong, W.-Q. Wang, F. Li, and H. C. So, "Sparsity-aware transmit beamspace design for FDA-MIMO radar," *Signal Process.*, vol. 144, pp. 99–103, Mar. 2018.

[40] J. Xu, G. Liao, Y. Zhang, H. Ji, and L. Huang, "An adaptive range-angle-Doppler processing approach for FDA-MIMO radar using three-dimensional localization," *IEEE J. Sel. Topics Signal Process.*, vol. 11, no. 2, pp. 309–320, Mar. 2017.

[41] F. van Belzen, S. Weiland, and J. de Graaf, "Singular value decompositions and low rank approximations of multi-linear functionals," in *Proc. 46th IEEE Conf. Decis. Control*, Dec. 2007, pp. 3751–3756.

[42] T. G. Kolda and B. W. Bader, "Tensor decompositions and applications," *SIAM Rev.*, vol. 51, no. 3, pp. 455–500, Aug. 2009.

TENGXIAN XU was born in Henan, in 1996. He received the B.S. degree from Hainan University, Haikou, China, in 2019, where he is currently pursuing the M.S. degree in information and communication engineering. His research interests include array signal processing and MIMO radar.

XIANPENG WANG (Member, IEEE) was born in 1986. He received the M.S. and Ph.D. degrees from the College of Automation, Harbin Engineering University, Harbin, China, in 2012 and 2015, respectively. From 2015 to 2016, he was a full-time Research Fellow with the School of Electrical and Electronic Engineering, Nanyang Technological University, Singapore. He is currently a Professor with the School of Information and Communication Engineering, Hainan University, Haikou, China. He is the author of more than 100 papers published in related journals and international conference proceedings, and was a reviewer of more than 20 journals. His major research interests include communication systems, array signal processing, radar signal processing, and compressed sensing and its applications.

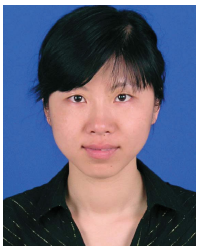

TING SU (Member, IEEE) received the B.S. degree in communication engineering and the Ph.D. degree in electronic science and technology from the Nanjing University of Science and Technology, Nanjing, China, in 2006 and 2016, respectively. She is currently a Postdoctoral Researcher with the Institute of Communications Engineering, Army Engineering University of PLA, Nanjing. She is also a Lecturer with Hainan University, Haikou, China. Her research interests include computational electromagnetic, radar signal processing, and wireless communications.

LIANGTIAN WAN (Member, IEEE) received the B.S. and Ph.D. degrees from the College of Information and Communication Engineering, Harbin Engineering University, Harbin, China, in 2011 and 2015, respectively. From October 2015 to April 2017, he was a Research Fellow with the School of Electrical and Electrical Engineering, Nanyang Technological University, Singapore. He is currently an Associate Professor with the School of Software, Dalian University of Technology, Dalian, China. He has authored or coauthored over 40 scientific papers in international journals and conferences. His current research interests include social network analysis and mining, big data, array signal processing, wireless sensor networks, and compressive sensing and its application. He has been serving as an Associate Editor for IEEE Access and *Journal of Information Processing Systems*.

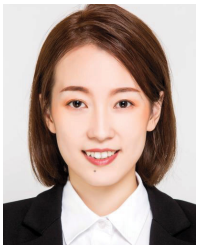

LU SUN received the B.S. and Ph.D. degrees with the School of Software from the Dalian University of Technology, Dalian, China, in 2013 and 2019, respectively. She is currently an Assistant Professor with the Institute of Information Science Technology, Dalian Maritime University, Dalian. Her current research interests include offshore communication, resource allocation, and wireless power transfer.